PAPER

# Nuclear acoustic envelope soliton in a relativistically degenerate magneto-rotating stellar plasma

To cite this article: Swarniv Chandra *et al* 2024 *Phys. Scr.* **99** 095613

Physica Scripta

PAPER

# Nuclear acoustic envelope soliton in a relativistically degenerate magneto-rotating stellar plasma

**Swarniv Chandra**[1,*], **Gobinda Manna**[2] and **Deepsikha Mahanta**[3]

[1] Department of Physics, Government General Degree College at Kushmandi, Dakshin Dinajpur, 733121, India
[2] Centre for Atmospheric Sciences, Indian Institute of Technology, Delhi; Hauz Khas, New Delhi 110016, India
[3] Department of Mathematics, Gauhati University, Guwahati, Assam 781014, India
[*] Institute of Natural Sciences and Applied Technology, Kolkata 700032, India.

**E-mail:** swarniv147@gmail.com

**RECEIVED**
29 January 2024

**REVISED**
11 July 2024

**ACCEPTED FOR PUBLICATION**
25 July 2024

**PUBLISHED**
28 August 2024

**Keywords:** nuclear acoustic wave, degenerate matter, nonlinear schrodinger equation, breather modes, phase portraits

## Abstract

The study explores a model called Relativistic Degenerate Magneto-Rotating Quantum Plasma (RDMRQP), which comprises a static heavy nucleus, an inertial non-degenerate light nucleus, and warm non-relativistic or ultra-relativistic electrons. The focus is on observing the emergence of Nucleus-Acoustic Envelope Solitons (NAESs). Using the reductive perturbation method, a Nonlinear Schrödinger equation (NLSE) is derived to characterize the properties of NAESs. We have analysed the Peregrine breather soliton solution. The investigation reveals that the temperature of warm degenerate species, plasma system's rotational speed, and the presence of heavy nucleus species can alter the fundamental features (height and width) of NAESs in the WDMRQP system. The study emphasizes the existence of only positive NA wave potential. Additionally, a phase plane analysis is conducted to gain a deeper understanding of the parametric dependencies. Through detailed mathematical and numerical analysis, the study avoids overloading with complex mathematics while demonstrating parametric dependence via phase portrait analysis. The research augments the envelop soliton model with breather mode solutions and discusses modulation instability using the Benjamin-Feir Index, highlighting the significance of solitons in star formation. Envelop solitons, stable waves within stars and proto-stars, influence energy transport and stellar evolution, playing a crucial role in the accretion process and formation of stable structures. Key findings include the effects of various parameters on NAESs' generation and propagation in which non-relativistic and ultra-relativistic electrons support NAESs, with amplitude and width influenced by temperature, rotational frequency, inclination angle, and the presence of a static heavy nucleus. The research is applicable to hot white dwarfs and neutron stars, suggesting further exploration of quantum effects and non-planar or arbitrary amplitude NAESs.

## 1. Introduction

Rotational motion of plasma is crucial in astrophysics, significantly impacting the behavior and evolution of celestial bodies. In stars, it affects their structure and magnetic activity, while in accretion disks around black holes and neutron stars, it drives intense radiation and relativistic jets. During star formation, rotation within molecular clouds leads to protostellar disks, essential for star and planetary system birth. Understanding rotating plasma dynamics provides insights into galactic structures and interstellar matter. Also in laboratories, magnetically confined rotating plasma is vital for nuclear fusion research. Magnetic confinement in devices like tokamaks and stellarators enhances stability and performance, emulating stellar fusion processes. Additionally, studying relativistically degenerate plasma informs the dynamics of stellar collapse, neutron star structure, and supernova events. Astrophysical jets manifest across various scales, from the early phases of star formation to the late stages of dying massive stars and compact objects [1]. They are observed in phenomena such as supernovae,

gamma-ray bursts, pulsars, pre-planetary nebulae, planetary nebulae, and microquasars [2–9]. The engines of gamma-ray bursts [10, 11], microquasars [12], and active galactic nuclei power these relativistic jets. Despite extensive observations, spatially resolved jet observations below certain scales remain scarce, with recent exceptions like the M87 jet observed by the Event Horizon Telescope [13]. Understanding jet physics involves three main regimes: engine and launch, propagation and collimation, and dissipation and particle acceleration. Magnetic fields are crucial in transferring energy and collimating jets, especially in the launch region. Various magnetically dominated mechanisms influence particle acceleration and jet behavior. Experimental plasma physics explores nucleus-acoustic waves in relativistic degenerate magneto-rotating plasma, relevant to environments like white dwarfs and neutron stars.

In the past, it was widely believed that the core of white dwarfs exclusively comprised helium nuclei. However, subsequent observations revealed the presence of carbon or oxygen nuclei in their cores. White dwarfs consist of degenerate electron species, lighter nuclear species (hydrogen isotopes), and heavier nuclear species (carbon or oxygen). The electrons are relativistically degenerate in the inner core and non-relativistically degenerate in the outer mantle [14]. This study investigated nucleus-acoustic envelope solitary structures in a magneto rotating plasma (MRP) with strongly coupled non-degenerate heavy nuclei, weakly coupled degenerate light nuclei, and weak-relativistically (or ultra-relativistically) degenerate electrons [15]. The Nonlinear Schrodinger equation, describing the evolution of the envelope solitary structures was analytically derived and numerically solved in a magnetised rotating, multi-component degenerate magneto plasma system [16, 17]. The strong interaction among heavy nuclear species is suggested by some authors as the source of dissipation, leading to the formation of nucleus-acoustic shock structures (NASS) with electrostatic and gravitational potentials [18–20]. Recent research has further explored amplitude-modulated heavy nucleus-acoustic envelope solutions (HNAESs) in a degenerate relativistic magneto rotating plasma (DRMRP) system [21], considering relativistically degenerate electrons, light nuclei, and non-degenerate mobile heavy nuclei. The cubic nonlinear Schrödinger equation and a dispersion relation for heavy nucleus-acoustic waves (HNAWs) were derived in this context. Additionally, phase plane analysis have been conducted on the nonlinear Schrodinger equation (NLSE) to understand the effect of parameters on the stability. We are motivated to study this problem on the following grounds: (i) All stellar bodies rotate about an axis. Sometimes they are along the magnetic field direction but in most cases it is aligned at an angle, (ii) in nuclear reactors, tokamaks, stellarators etc the orbit of rotation of plasma particles are aligned obliquely with magnetic field or they themselves get disoriented during rotation.

We investigate the dynamics of linear nucleus-acoustic waves within a relativistic degenerate magneto rotating plasma system (DMRP) characterized by strong coupling. This system comprises strongly coupled non-degenerate heavy nuclei like metal nuclei, weakly coupled degenerate non-relativistic light nuclei like hydrogen, helium, lithium etc, and non-relativistically or ultra-relativistically degenerate electrons. Our focus is on a study of amplitude modulation and formation of envelope solitons. Through a linear perturbation analysis, we explore the nature of the instability associated with nucleus-acoustic waves in this degenerate magneto rotating plasma system. Heavy nuclei are almost immobile when compared to electrons and their density is also low due to the plasma under consideration have lesser heavy nuclei that take part in the dynamics of the system in consideration.

In our model, nucleus-acoustic waves manifest as propagating longitudinal oscillations resulting from the combined effects of inertia from the heavy nuclei and elasticity contributed jointly by the relativistic degeneracy pressure of lighter electrons and the classical thermal pressure of lighter nuclei. It's worth noting that the thermal pressure from the lighter nuclei is significantly smaller than its electronic counterpart. Consequently, the nucleus-acoustic wave is solely driven by the interaction between heavy nuclei (as inertial species) and degenerate electrons (as thermal species), giving rise to a phase velocity for the longitudinal oscillations to propagate as ($v_p$). This coupling of dynamics between heavy nuclei and degeneracy pressure is expressed in a closed form. The strong coupling of non-degenerate heavy nuclei is a result of their high charge and extremely low temperature, leading to a 'coupling parameter' much larger than unity, indicative of viscoelastic behavior which can be of great importance in compact astrophysical environments with high population density and low temperature, such as white dwarfs and neutron stars. The physicality of the problem can be understood from the works on star formation, planetary jets etc [1, 3, 8, 12, 13].

Keeping in mind the the scope of the journal and to retain the 'physics' part of our finding we do not include too much of mathematics in the text body. We prefer keeping the article crisp and physics oriented. The paper is organised in the following manner. In section 2 we present the model equations. In the next section (3) we carry out the linear and nonlinear analysis. The derivation and the solution of the Nonlinear Schrodinger equation (NLSE) is presented in the sections 3.2, 3.3 and 3.4. In subsequent section 4 we present the phase plane analysis and study the parametric dependence for different cases. Finally we conclude the findings in section 5. In a nutshell the motivation behind the work is to study the dependence of alignment of the rotational axis with the magnetic axis, the speed of rotation and the relative composition of the multi nuclear plasma.

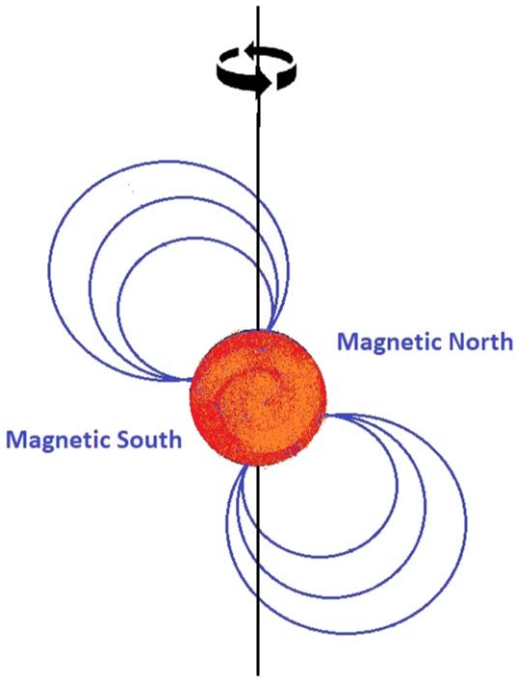


**Figure 1.** Schematic diagram of a rotating star and its magnetic field orientation with respect to the spin axis.

## 2. Model and governing equations

We examine a Rotating Degenerate Magnetized Rotating Plasma (RDMRP) system comprising an immobile heavy nucleus with low density, an inertial non-degenerate light nucleus, and a warm degenerate electron to investigate the fundamental characteristics of Nucleus-Acoustic Surface Waves (NASWs). In this plasma system (figure 1), a rotational magnetic field ($\vec{B} = B_0\vec{z}$) is present, oriented at an angle $\theta$ around the $z$-axis. The charge neutrality condition for this three-dimensional magneto-rotating degenerate plasma is expressed as $Z_h n_{h0} + Z_l n_{l0} \approx n_{e0}$, where $Z_h$, $Z_l$, $n_{h0}$, $n_{l0}$ and $n_{e0}$ represent the charge state of the heavy nucleus, charge state of the light nucleus, unperturbed number density of the heavy nucleus, unperturbed number density of the light nucleus, and unperturbed number density of electrons, respectively. It is important to note that the heavy nucleus has a considerably lower number density compared to the light nucleus and electrons. Moreover, in this degenerate plasma system, the heavy nucleus is assumed to be static and immobile due to its low number density. The dynamics of nonlinear Nucleus-Acoustic waves are described by a set of normalized equations [22]:

$$\frac{\partial n_l}{\partial t} + \vec{\nabla} \cdot (n_l \vec{u}_l) = 0, \tag{1}$$

$$\left(\frac{\partial u_l}{\partial t} + (\vec{u}_l \cdot \vec{\nabla})\vec{u}_l\right) = -\vec{\nabla}\phi + \omega_{cl}(\vec{u}_l \times \hat{z}) + 2(\vec{u}_l \times \vec{\omega}_r), \tag{2}$$

$$\nabla^2\phi = (1 + \delta)n_e - n_l - \delta. \tag{3}$$

The normalization scheme is given in the appendix. $\omega_{cl}$ & $\omega_r$ are the light nuclear cyclotron frequency and the rotational frequency of the star respectively. $\delta$ is the ratio of heavy nuclear charge density to that of lighter nuclei given by:

$$\delta = \frac{Z_h n_{h0}}{Z_l n_{l0}}. \tag{4}$$

## 3. Linear and nonlinear analysis

### 3.1. Linear dispersion relation

In order to obtain the evolutionary equation which leads to the formation of envelope soliton we employ multiple scale perturbation theory. For this we use stretching of the space and time coordinates as:

$$\xi = \epsilon^{\frac{1}{2}}(l_x x + l_z z - \lambda t) \quad \& \quad \tau = \epsilon^{\frac{3}{2}} t. \tag{5}$$

We next use the standard technique of using Fourier series expansion coupled with perturbation series. Separating sets of equation corresponding to different harmonics and within them terms with similar order of perturbation we obtain the nonlinear Schrodinger equation (NLSE) [23, 24]. Derivation of the 1d nonlinear Schrödinger equation from the 3d many-body plasma dynamics is qualitatively equivalent to study the 3-D problem. Such a process helps to reduce the mathematical rigours without losing much information. The outline of the derivation is redundant and can be found in the literature [25–28].

The generalised Fourier expansion and perturbations are given as:

$$f = f_0 + \sum_s [f_s \exp(is\psi) + f_s^* \, exp(-is\psi)]. \tag{6}$$

Here $f_s$ is the *sth* harmonic of the field quantity 'f' which can be velocity, density, potential etc $f_s^*$ is the complex conjugate of $f_s$. The different harmonic quantities are separated from the set of normalised and scalarised governing equations. The different harmonic field quantities are further expanded via a general perturbation series given by:

$$f_s = f_{s0} + \varepsilon^{p_1} f_{s1} + \varepsilon^{p_2} f_{s2} + \varepsilon^{p_3} f_{s3} + ..... \tag{7}$$

Here $p_j$'s can be integral (odd or even) or fraction (successive or skipping) depending upon the strength and nature of perturbations.

After series of algebraic exercise and sorting of ordered terms one finally obtains the linear dispersion relation from the lowest order terms in $\epsilon$ given by

$$\omega = k + C_1 k^3 + C_2 k^5 + C_3 k^7. \tag{8}$$

Here the coefficients are given as:

$$C_1 = -3\left[\left(\frac{\gamma k_{Te}}{2+2\delta}\right)\left\{1 + \frac{l_x^2}{\tilde{\omega}_l^2}\left(1 - 2\frac{l_z\omega_0}{l_x\tilde{\omega}_l}\,\mathrm{Sin}\,\theta\right)\right\}\right];$$

$$C_2 = \frac{9}{10}\left[\left(\frac{\gamma k_{Te}}{2+2\delta}\right)\left\{1 + \frac{l_x^2}{\tilde{\omega}_l^2}\left(1 - 2\frac{l_z\omega_0}{l_x\tilde{\omega}_l}\,\mathrm{Sin}\,\theta\right)\right\}\right]^2;$$

$$C_3 = -\frac{27}{42}\left[\left(\frac{\gamma k_{Te}}{2+2\delta}\right)\left\{1 + \frac{l_x^2}{\tilde{\omega}_l^2}\left(1 - 2\frac{l_z\omega_0}{l_x\tilde{\omega}_l}\,\mathrm{Sin}\,\theta\right)\right\}\right]^3$$

### 3.2. Nonlinear schrodinger equation

Going to the higher order terms in $\epsilon$ one obtains the NLSE as:

$$i\frac{\partial\phi}{\partial\tau} + D\frac{\partial^2\phi}{\partial\xi^2} = N(\phi^2\phi^*). \tag{9}$$

where D and N are dispersive and nonlinear coefficients given by:

$$D = -3k\left[\left(\frac{\gamma k_{Te}\lambda}{2+2\delta}\right)\left\{1 + \frac{l_x^2}{\tilde{\omega}_l^2}\left(1 - 2\frac{l_z\omega_0}{l_x\tilde{\omega}_l}\,\mathrm{Sin}\,\theta\right)\right\}\right]$$

$$N = -\frac{\lambda^2}{24\cdot k}\left[2(1+\lambda)\frac{1+\delta}{\gamma_e k_{Te}} - \frac{2-\gamma_e}{\gamma_e k_{Te}}\right]^2\left[\frac{\gamma_e k_{Te}\lambda}{2(1+\delta)}\right]^{-1}\left[1 + \frac{l_x^2}{\tilde{\omega}_l^2}\left(1 - 2\frac{l_z\omega_0}{l_x\tilde{\omega}_l}\,\mathrm{Sin}\,\theta\right)\right]^{-1}$$

The nonlinear Schrödinger equation (NLSE) is a fundamental equation in quantum mechanics that describes the behavior of wave functions in nonlinear systems. There are various types of solutions to the NLSE, each revealing distinct physical phenomena.

(i) *Soliton Solutions:* Solitons are stable, localized wave packets that maintain their shape and amplitude during propagation. They arise due to a balance between dispersion and nonlinearity.

(ii) *Breather Solutions:* Breathers are a subclass of solitons characterized by periodic oscillations in amplitude and width. They represent localized excitations within a continuous wave background [29, 30].

(iii) *Modulational Instability Solutions:* This type of solution describes the growth of perturbations in the wave amplitude over time, leading to the formation of localized structures.

(iv) *Stationary States:* These solutions represent stable, time-independent states where the wave function does not evolve with time.

Understanding and manipulating these solutions are crucial for applications in various fields, including optics, plasma physics, and condensed matter physics.

### 3.3. Breather mode solution

The breather solution of the nonlinear Schrödinger equation (NLSE) represents a fascinating phenomenon in the realm of nonlinear dynamics and quantum mechanics. Unlike standard solutions, breathers are localized and time-periodic structures that can persist in certain nonlinear systems. These solutions emerge due to the delicate balance between dispersion and nonlinearity in the NLSE. The breather's unique characteristics include its ability to oscillate without spreading, forming a breather 'packet.' This localized, pulsating wave pattern is a result of the interplay between attractive and repulsive forces within the nonlinear medium. Since breather solutions contributes to insights in diverse fields, including optics, condensed matter physics, and plasma physics we therefore keeping in mind our plasma problem into consideration investigate the Breather solution. In this work we focus on the Peregrine breather mode and the Modulational Instability. Analytic solution of the NLSE as given by Peregrine (Peregrine breathers)

$$\phi(\xi,\,\tau) = \sqrt{\frac{2D}{N}}\left[\frac{4(1\,+\,4iD\tau)}{1\,+\,16D^2\tau^2\,+\,4\xi^2}\,-\,1\right]\exp(2iD\tau). \tag{10}$$

In the subsequent figures we will show the evolutionary stages of Peregrine breather modes (figure 2) and its spatial and temporal variations (figure 3). We also study the obliquity dependence (figure 4) for weakly relativistic case and $\delta$ (heavy nuclear charge density to that of lighter nuclei) dependence (figure 5) for ultra relativistic case. These two cases are important because obliquity has effectively no influence on ultra relativistic case and nuclear charge density for heavy and light nuclei has almost equal roles to play in weakly relativistic case. The units are in normalised framework and since a hybrid normalization is used sometimes they are more than unity. The hybrid normalization is justified since we are interested to observe some details of the mechanisms and its dependence.

From the figure 2 we see that the Peregrine breather solitons corresponding to ultra-relativistic degenerate plasma has a spread out temporal domain (a)–(b) when compared to weakly relativistic case (c)–(d) suggesting less influence of dispersive factors. However in the case of spatial dependence of dispersive effects, the ultra-relativistic case is narrowed out suggesting an almost non-changing breather width. When compared to figures (e–f) which correspond to thermal degeneracy, we find that the dispersion is mainly spatial. To get a clear picture of our evolutionary mechanism we provide a 2-D depiction in figure 3. The temporal and spatial cross sections are shown in sub-figures (a)–(f) respectively. We see that the nonlinear effect is maximum initially and flattens out as both space and time increases. This is relatable with the nature of breather solitons. These figures make it easy to understand the dependence of dispersive and nonlinear factors on space and time.

### 3.4. Modulational instability and the Benjamin Feir Index

In the preceding section we have investigated the breather mode solutions for ultra & weakly relativistic case and compared them with the classical case. Now, under certain situations and those with starting from a plane wave and evolving into an envelop soliton solution whose amplitude is given by:

$$\eta(\xi,\,\tau) = \frac{1}{2}[\phi(\xi,\,\tau)e^{(k_c\xi-\omega_c\tau)}\,+\,c.c.] \tag{11}$$

Here $\omega_c$ and $k_c$ are the frequency and the magnitude of the wave-vector of the carrier wave respectively and $\phi(\xi,\tau)$ is the slowly varying complex envelope. In this respect it becomes important to introduce the Benjamin-Feir Index (BFI) expressed as:

$$BFI = \sqrt{\Gamma} = \left|\frac{N{\phi_0}^2}{(\Delta\omega)^2 D}\right|^{1/2}. \tag{12}$$

Here $\Delta\omega$ is the initial spectral bandwidth evaluated at $\tau = 0$. Taking time average of the quantities we find $\langle\eta^2(\xi,\,\tau)\rangle = \left\langle\frac{\phi^2(\xi,\,\tau)}{2}\right\rangle$. It can be seen that large values of BFI lead to the formation of rogue waves which are characterized by a heavy-tailed statistical distributions modulated waveform.

The strength of nonlinearity can be judged from the value f this BFI. To give a qualitative flavor of how this parameter helps in measuring nonlinearity let us define two time scales given by: $\tau_{lin} = D(\Delta\omega)^2$ & $\tau_{non-lin} = N^{-1}(\phi_0)^2$ The degree on nonlinearity of the propagating wave an thus be given by the BFI in the ratio of these two time scales as:

$$BFI = \sqrt{\Gamma} = (\tau_{lin}/\tau_{non-lin})^{1/2}. \tag{13}$$

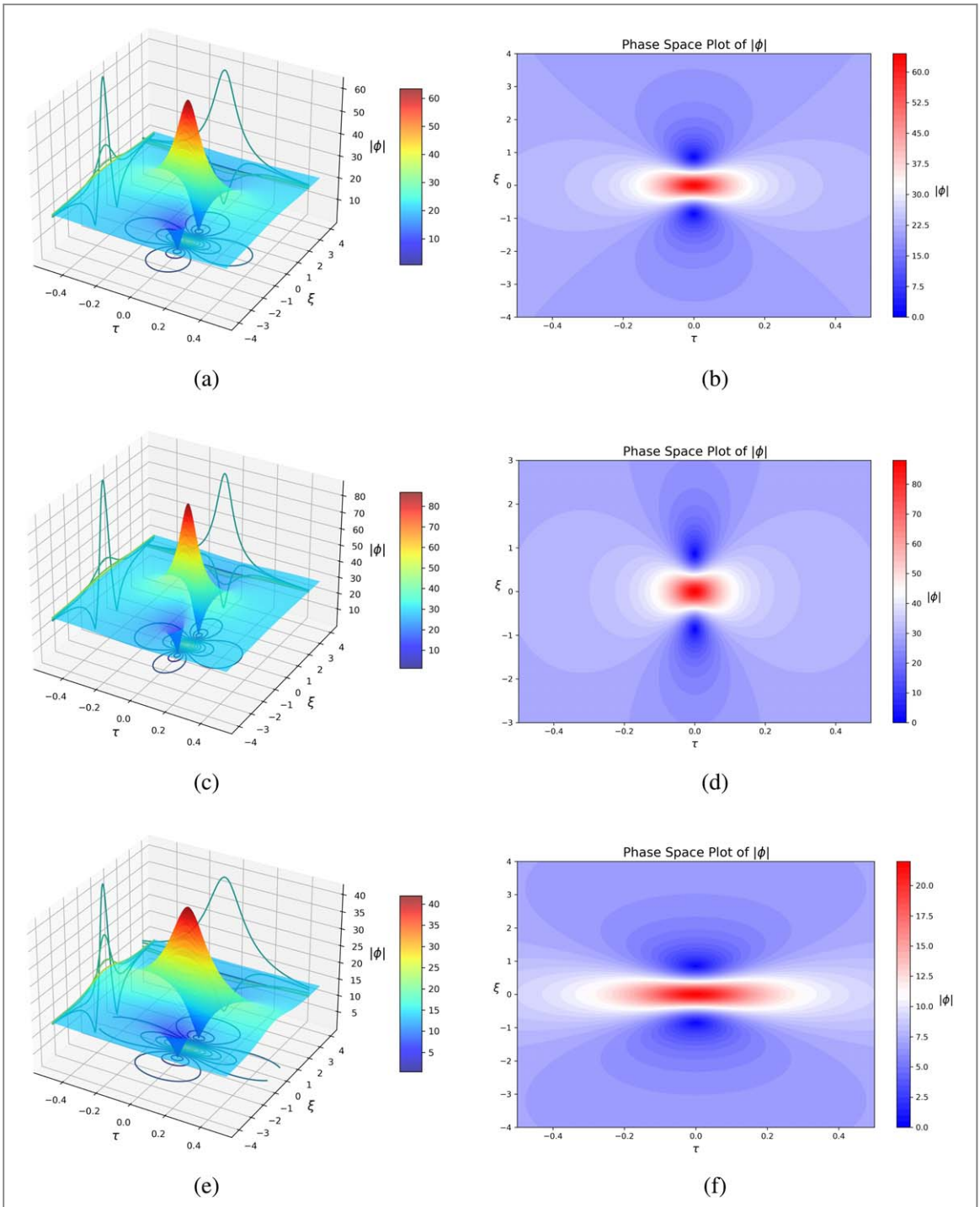


**Figure 2.** Peregrine breather modes and its contour plots for ultra-relativistic case (a), (b); weakly relativistic case (c), (d) and comparison with classical case (e), (f).

Or in terms of the carrier wave wavenumber ($k_0$) as:

$$BFI = \sqrt{\Gamma} = \frac{\epsilon}{\Delta\omega/\omega_0}. \tag{14}$$

Here $\epsilon = k_0\sqrt{2I}$, $I$ being the intensity of the modulated waveform. We present this section in order to relate this type of theoretical work with experimental observations and associated parameters.

## 4. Phase plane analysis & parametric dependence

Phase plane analysis is a valuable tool in understanding the behavior and stability of plasma systems, commonly used in fusion research. In the context of plasma physics, a phase plane typically represents the evolution of two

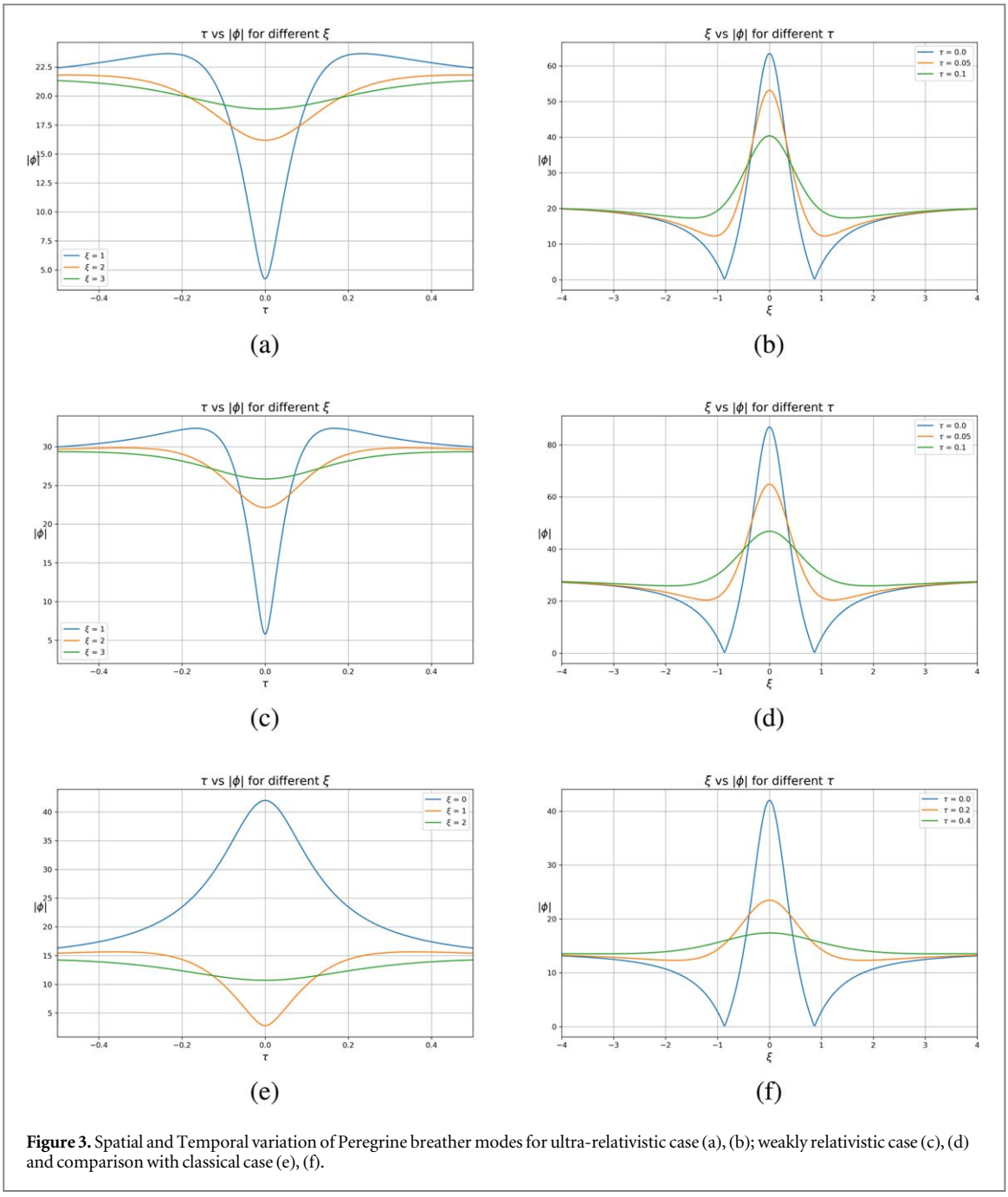


**Figure 3.** Spatial and Temporal variation of Peregrine breather modes for ultra-relativistic case (a), (b); weakly relativistic case (c), (d) and comparison with classical case (e), (f).

relevant variables, such as plasma density and temperature. Stability criteria in plasma systems are crucial for ensuring controlled and sustainable fusion reactions.

Researchers employ phase plane analysis to study trajectories of plasma states and identify equilibrium points. Stability is assessed by examining how small perturbations from these equilibrium points evolve over time. Common stability criteria involve the consideration of Lyapunov stability, where trajectories either converge to stable fixed points or diverge from unstable ones.

In plasma physics [31–33], stability analysis informs the design and operation of magnetic confinement devices like tokamaks. Understanding the phase plane behavior and applying stability criteria contribute to the development of effective strategies for achieving and maintaining stable plasma conditions in fusion experiments.

We convert or nonlinear Schrodinger equation into a set of dynamical systems (DS) equations. The transformation and the DS are given here. We use transformation of variables $\zeta$ and $\phi$ as $\zeta = l_x\xi - M\tau$ with $M = \omega_c/k_c$ and $\phi(\zeta) = \psi(\zeta)exp(i\beta\zeta)$, with $\beta$ as a phase factor the NLSE takes the form of

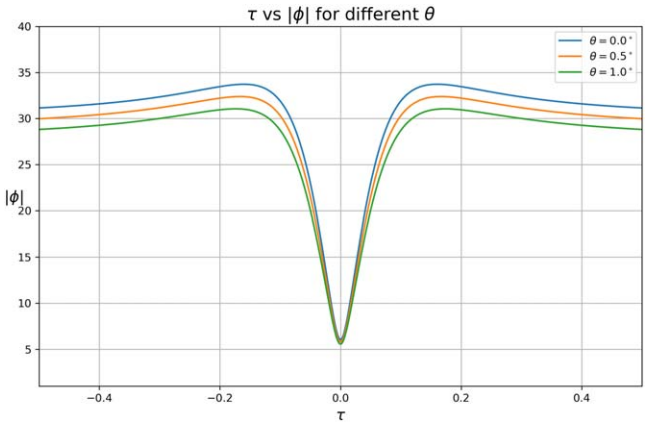


**Figure 4.** Variation of breather amplitude with angle of inclination in the weakly relativistic case. Here $\sigma_{Te} = 0.2, \sigma_e = 0.2, k = 0.2, l_x = 0.2, \gamma = \frac{5}{3}, \omega_0 = 0.03, \delta = 0.3$.

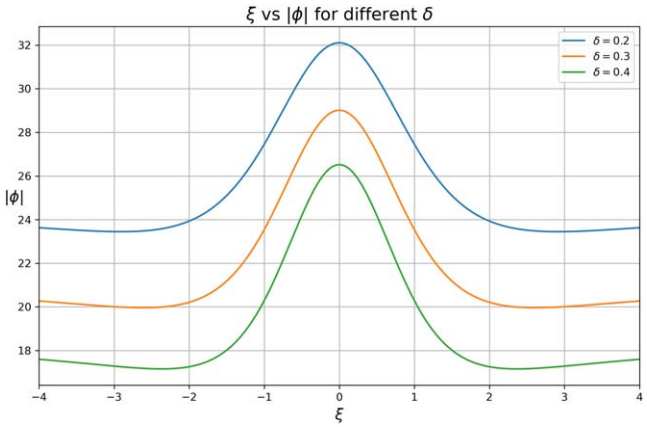


**Figure 5.** Variation of breather amplitude with heavy to light nuclear charge density ratio ($\delta$) in the ultra relativistic case. Here $\sigma_{Te} = 0.2, \sigma_e = 0.2, k = 0.2, l_x = 0.2, \gamma = \frac{5}{3}, \omega_0 = 0.03, \theta = 5^\circ$.

$$\frac{\partial^2\psi}{\partial\zeta^2} = \left(\beta^2 - \frac{1}{Dl_x{}^2}\beta M\right)\psi + \frac{N}{Dl_x{}^2}\psi^3. \tag{15}$$

Upon integrating twice with eta with boundary conditions the dynamical system equations are written as,

$$\frac{\partial\psi}{\partial\zeta} = \mathrm{z}. \tag{16}$$

$$\frac{\partial \mathrm{z}}{\partial\zeta} = F_1\psi - F_2\psi^3. \tag{17}$$

Where $F_1$ and $F_2$ are defined as below

$$\mathrm{F_1} = \left[\beta^2 - \frac{1}{P}\beta\mathrm{M}\right] \quad \& \quad \mathrm{F_2} = -\frac{Q}{P}. \tag{18}$$

And the field s given as:

$$F = (\mathrm{z},\ \mathrm{F_1}\psi - \mathrm{F_2}\psi^3). \tag{19}$$

The field will be conservative if $\vec{\nabla}\dot{F} = 0$ and the Hamiltonian is given by,

$$\mathrm{H} = \frac{z^2}{2} - \frac{F_1\psi^2}{2} + \frac{F_2}{4}\psi^4. \tag{20}$$

In the following figures we present the phase portraits corresponding to different cases to study the dependence of dynamical system equations corresponding to NLSE on various plasma parameters and draw

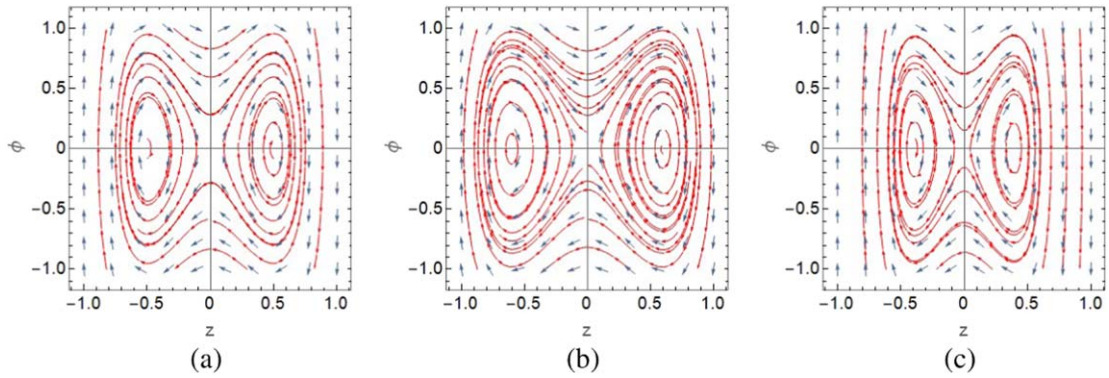


**Figure 6.** Phase portraits of the NLSE in case of (a) ultra-relativistic ($\gamma = 4/3$), (b) weakly-relativistic ($\gamma = 5/3$) and (c) classical ($\gamma = 1$) cases. Here $\sigma_{Te} = 0.2, \sigma_e = 0.2, k = 0.2, l_x = 0.2, \theta = 5^\circ, \omega_0 = 0.03, \delta = 0.3$.

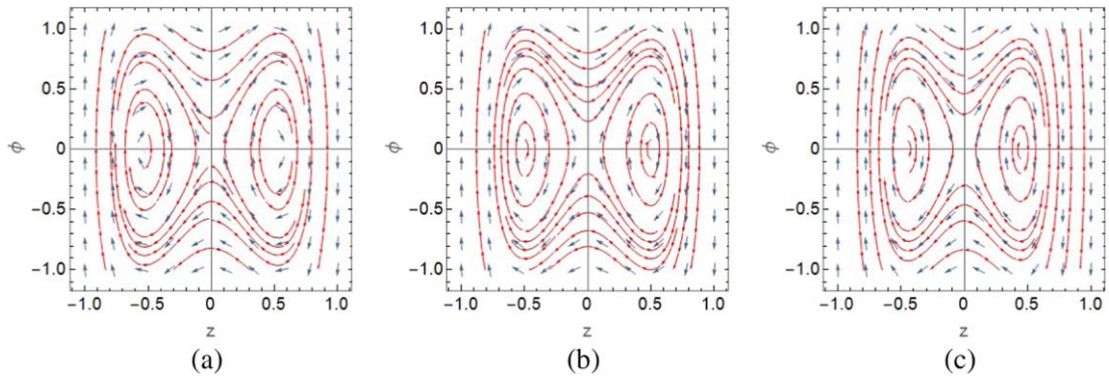


**Figure 7.** Phase portraits of the NLSE in case of ultra-relativistic case for different values of $\sigma_{Te}$; (a) $\sigma_{Te} = 0.1$, (b) $\sigma_{Te} = 0.2$ and (c) $\sigma_{Te} = 0.3$ Here $\sigma_e = 10, k = 0.2, l_x = 0.2, \theta = 5^\circ, \omega_0 = 0.03, \delta = 0.3$.

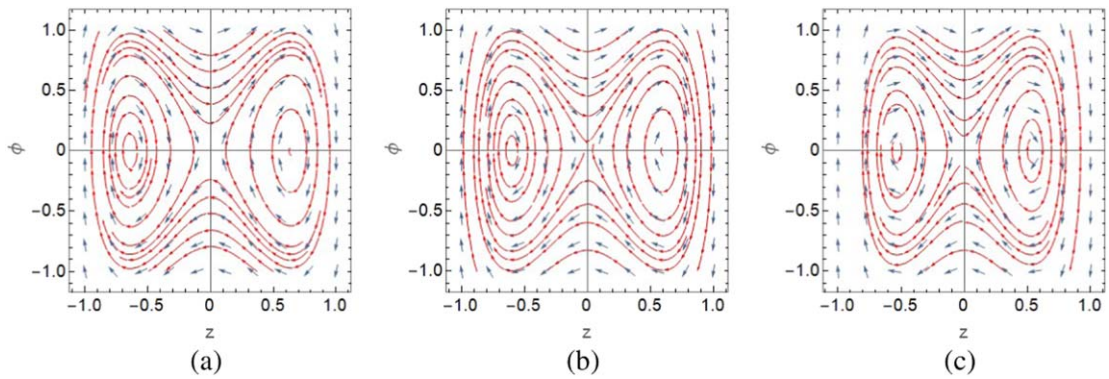


**Figure 8.** Phase portraits of the NLSE in case of weakly-relativistic case for different values of $\sigma_{Te}$; (a) $\sigma_{Te} = 0.1$, (b) $\sigma_{Te} = 0.2$ and (c) $\sigma_{Te} = 0.3$ Here $\sigma_e = 10, k = 0.2, l_x = 0.2, \theta = 5^\circ, \omega_0 = 0.03, \delta = 0.3$.

valuable information from them. The figures and their captions are sufficient to explain the parametric dependence. To contain the volume of our manuscript we do not carry out any individual discussions on the dynamical system plots, i.e. the phase portraits.

In figure 6 we see the phase portraits corresponding to the DS equations in ultra-relativistic (UR), weak-relativistic (WR) and classical case. While there are evidence of limit cycle and fixed points, the separation of the fixed points differ in case of ultra-relativistic, weak-relativistic and classical cases. The effect of thermal energy to Fermi energy ratio ($\sigma_{Te}$) and ratio of rest energy to Fermi energy ($\sigma_e$) for ultra relativistic and weakly relativistic cases are shown in figures 7–10 respectively.

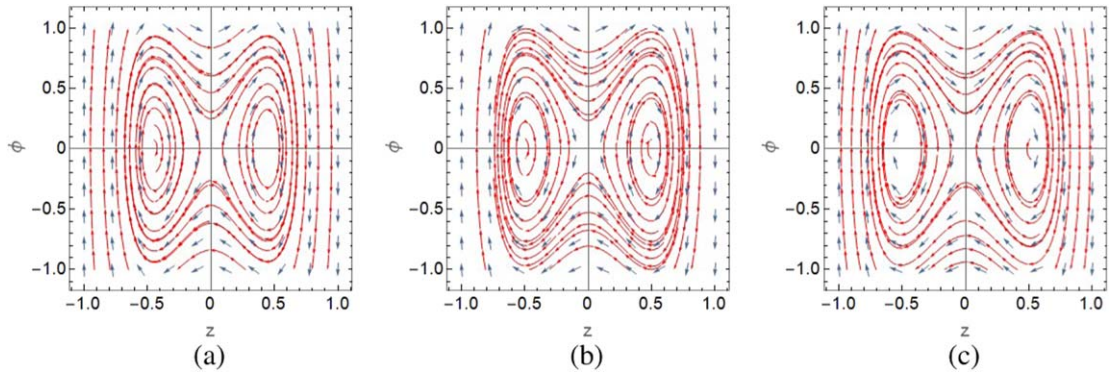


**Figure 9.** Phase portraits of the NLSE in case of ultra-relativistic case for different values of $\sigma_e$; (a) $\sigma_e = 5$, (b) $\sigma_e = 10$ and (c) $\sigma_e = 15$ Here $\sigma_{Te} = 0.2, k = 0.2, l_x = 0.2, \theta = 5^\circ, \omega_0 = 0.03, \delta = 0.3$

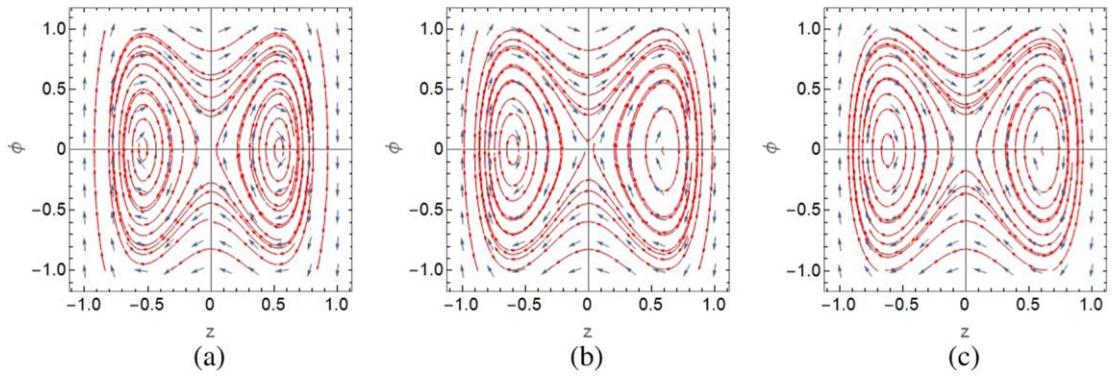


**Figure 10.** Phase portraits of the NLSE in case of weakly-relativistic case for different values of $\sigma_e$; (a) $\sigma_e = 5$, (b) $\sigma_e = 10$ and (c) $\sigma_e = 15$ Here $\sigma_{Te} = 0.2, k = 0.2, l_x = 0.2, \theta = 5^\circ, \omega_0 = 0.03, \delta = 0.3$.

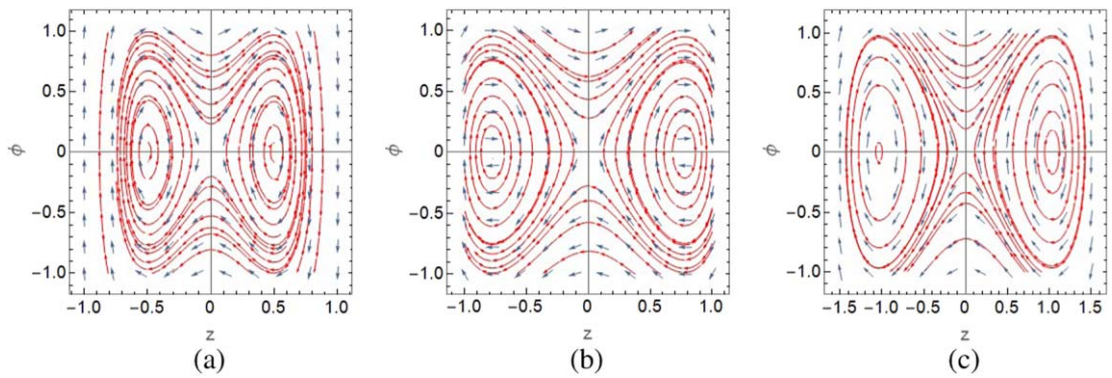


**Figure 11.** Phase portraits of the NLSE in case of ultra-relativistic case for different values of wavenumber (k); (a) $k = 0.2$, (b) $k = 0.4$ and (c) $k = 0.6$. Here $\sigma_{Te} = 0.2, \sigma_e = 10, l_x = 0.2, \theta = 5^\circ, \omega_0 = 0.03, \delta = 0.3$.

The effect of carrier wave wavenumber (k) for UR & WR cases are shown in figures 11 and 12. While in both cases the fixed points move wide apart, in case of UR situation the fixed points move rapidly away from each other. The angle of inclination of the plane of rotation with respect to the axes represented by the directional cosine ($l_x$) is instrumental in intensifying/weakening the strength of the attractors, it can not alter the position of the fixed points (figures 13 and 14). Further the orientation of the plane of rotation with respect to the magnetic axis represented by ($\theta$) (figures 15 and 16), the speed of rotation ($\omega_0$) (figures 17 and 18) and the heavy-to-light nuclear charge density ratio ($\delta$) (19 and 20) has some impact on the formation of envelop solitons respectively.

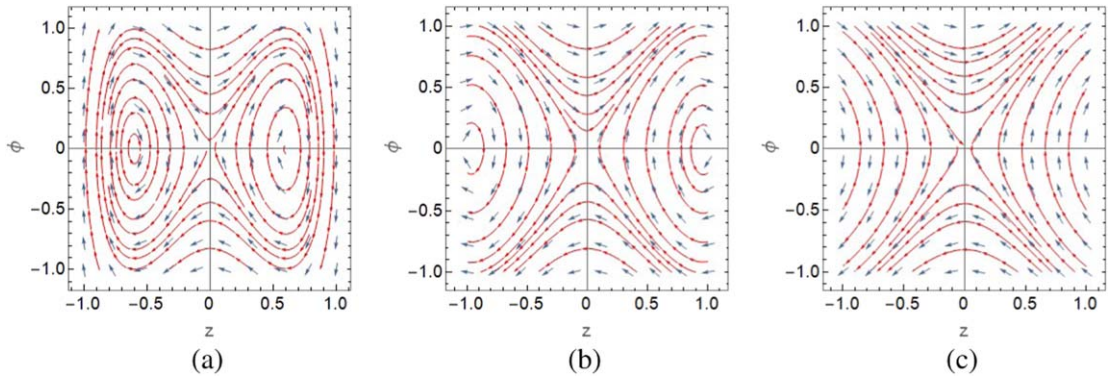


**Figure 12.** Phase portraits of the NLSE in case of weakly-relativistic case for different values of wavenumber (k); (a) $k = 0.2$, (b) $k = 0.4$ and (c) $k = 0.6$. Here $\sigma_{Te} = 0.2, \sigma_e = 10, l_x = 0.2, \theta = 5^\circ, \omega_0 = 0.03, \delta = 0.3$.

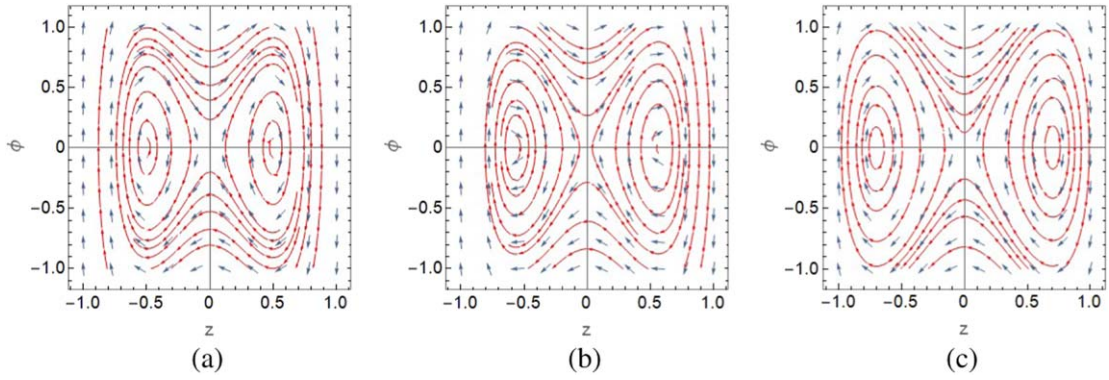


**Figure 13.** Phase portraits of the NLSE in case of ultra-relativistic case for different values of directional cosines ($l_x$); (a) $l_x = 0.2$, (b) $l_x = 0.4$ and (c) $l_x = 0.6$. Here $\sigma_{Te} = 0.2, \sigma_e = 10, k = 0.2, \theta = 5^\circ, \omega_0 = 0.03, \delta = 0.3$.

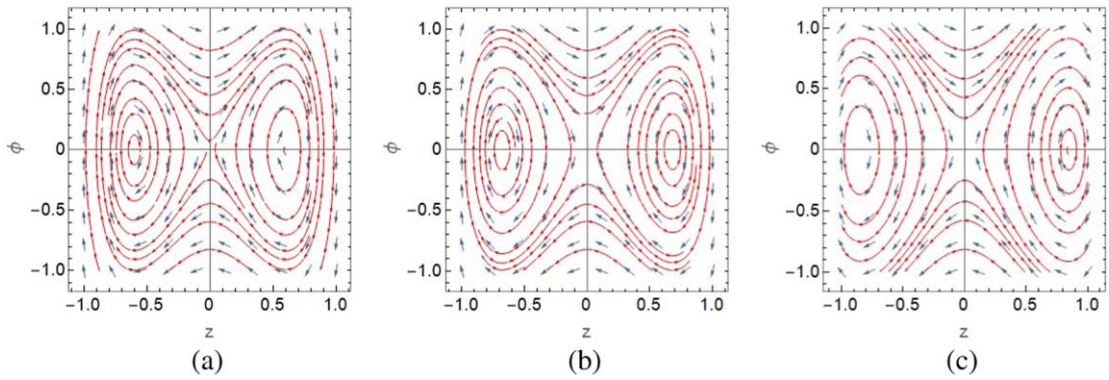


**Figure 14.** Phase portraits of the NLSE in case of weakly-relativistic case for different values of directional cosines ($l_x$); (a) $l_x = 0.2$, (b) $l_x = 0.4$ and (c) $l_x = 0.6$. Here $\sigma_{Te} = 0.2, \sigma_e = 10, k = 0.2, \theta = 5^\circ, \omega_0 = 0.03, \delta = 0.3$.

The magnetic field though crucial in confining the plasma, does not show significant changes in the nature and properties of the phase portraits.

### 4.1. Interpretation of phase plane analysis

The following figures illustrate the phase portraits of the Nonlinear Schrödinger equation (NLSE) for different cases: ultra-relativistic, weakly relativistic, and classical. Each figure contains three subfigures corresponding to

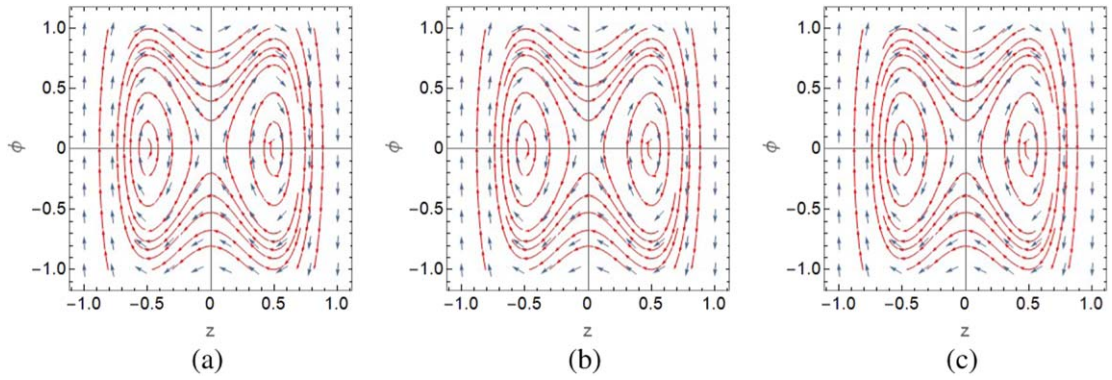


**Figure 15.** Phase portraits of the NLSE in case of ultra-relativistic case for different values of angle of inclination $\theta$; (a) $\theta = 3°$, (b) $\theta = 5°$ and (c) $\theta = 7°$. Here $\sigma_{Te} = 0.2, \sigma_e = 10, k = 0.2, l_x = 0.2, \omega_0 = 0.03, \delta = 0.3$.

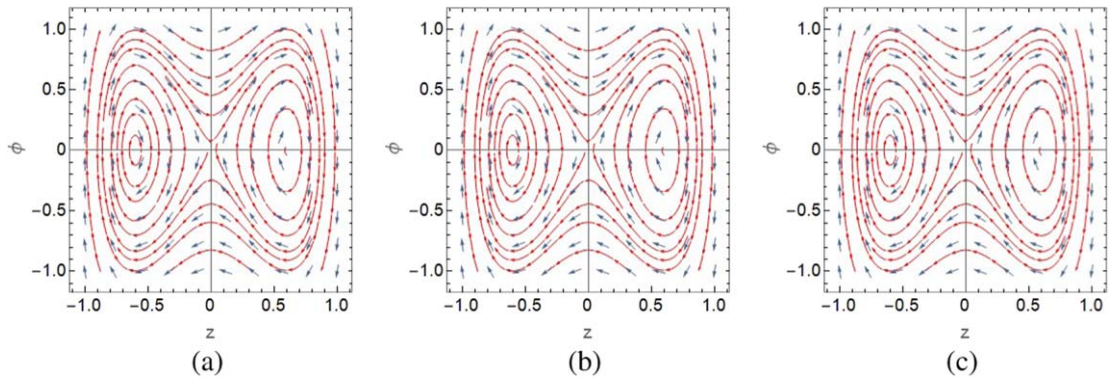


**Figure 16.** Phase portraits of the NLSE in case of weakly-relativistic case for different values of angle of inclination $\theta$; (a) $\theta = 3°$, (b) $\theta = 5°$ and (c) $\theta = 7°$. Here $\sigma_{Te} = 0.2, \sigma_e = 10, k = 0.2, l_x = 0.2, \omega_0 = 0.03, \delta = 0.3$.

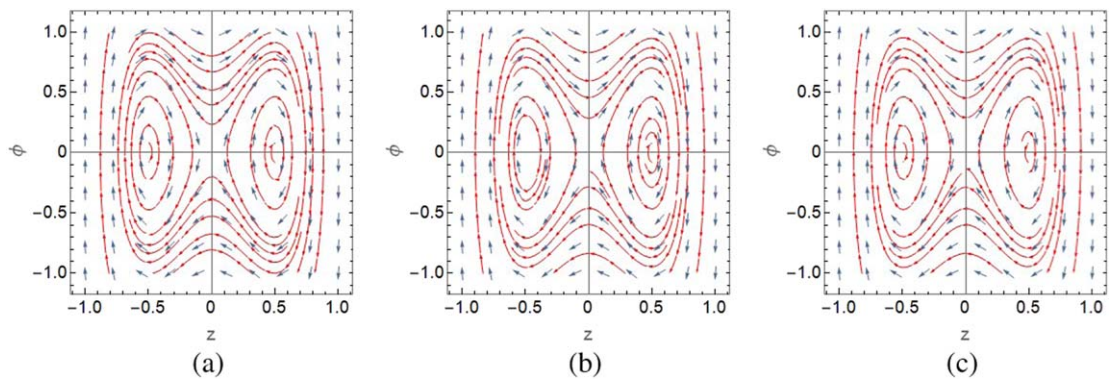


**Figure 17.** Phase portraits of the NLSE in case of ultra-relativistic case for different values of rotational frequency $\omega_0 = 0.03$; (a) $\omega_0 = 0.03$, (b) $\omega_0 = 0.05$ and (c) $\omega_0 = 0.07$. Here $\sigma_{Te} = 0.2, \sigma_e = 10, k = 0.2, l_x = 0.2, \theta = 5°, \delta = 0.3$.

these cases, highlighting the dynamical behavior of the system under varying plasma parameters. We explain them in point-wise manner. Figure 6 shows the Phase Portraits of the NLSE for different case. viz. Ultra-Relativistic Case ($\gamma = 4/3$), Weakly Relativistic Case ($\gamma = 5/3$) and Classical Case ($\gamma = 1$). Here other parameters are $\sigma_{Te} = 0.2, \sigma_e = 0.2, k = 0.2, l_x = 0.2, \theta = 5°, \omega_0 = 0.03, \delta = 0.3$ respectively. In each scenario, fixed points and limit cycles are evident, with notable differences in the separation of fixed points across the cases. Figures 7 and 8 the effect of $\sigma_{Te}$ (Thermal to Fermi Energy Ratio) is discussed for two cases:

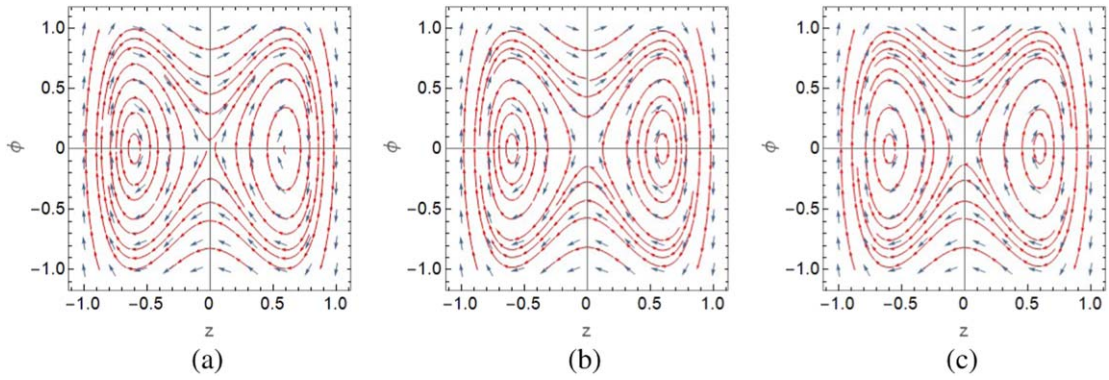


**Figure 18.** Phase portraits of the NLSE in case of weakly-relativistic case for different values of rotational frequency $\omega_0$; (a) $\omega_0 = 0.03$, (b) $\omega_0 = 0.05$ and (c) $\omega_0 = 0.07$. Here $\sigma_{Te} = 0.2, \sigma_e = 10, k = 0.2, l_x = 0.2, \theta = 5^\circ, \delta = 0.3$.

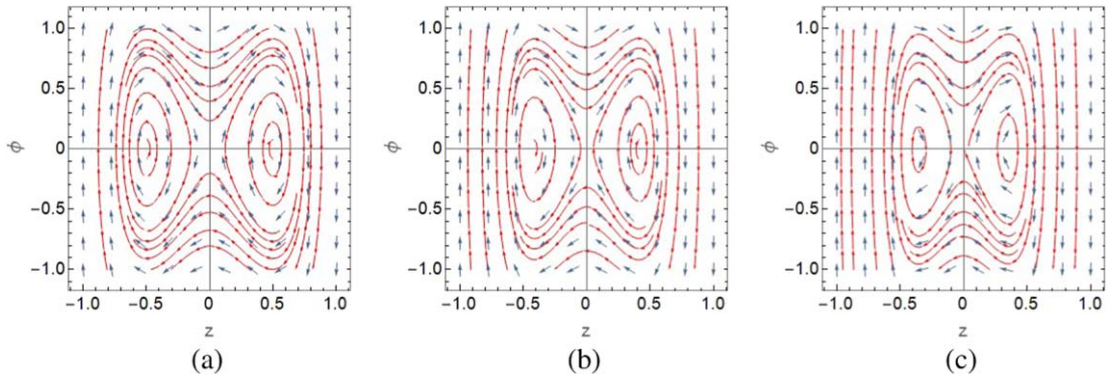


**Figure 19.** Phase portraits of the NLSE in case of ultra-relativistic case for different values of heavy-to-light nuclear charge density $\delta = 0.3$; (a) $\delta = 0.3$, (b) $\delta = 0.5$ and (c) $\delta = 0.7$. Here $\sigma_{Te} = 0.2, \sigma_e = 10, k = 0.2, l_x = 0.2, \theta = 5^\circ, \omega_0 = 0.03$.

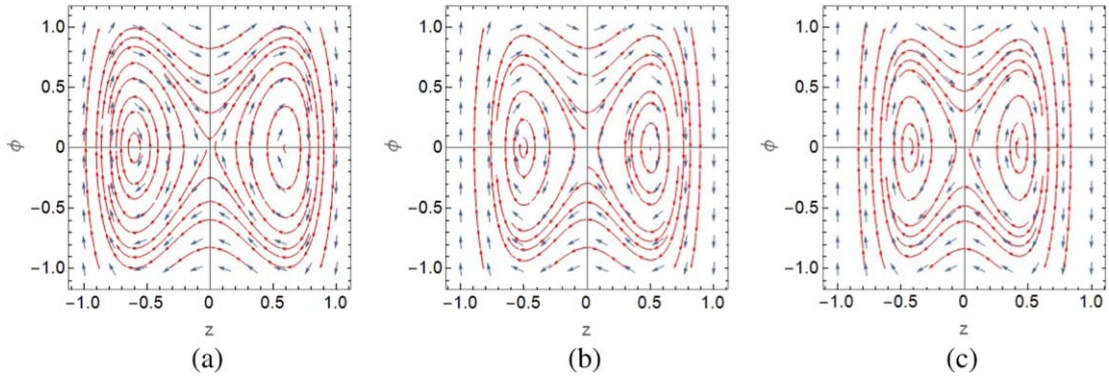


**Figure 20.** Phase portraits of the NLSE in case of weakly-relativistic case for different values of heavy-to-light nuclear charge density ratio $\delta = 0.3$; (a) $\delta = 0.3$, (b) $\delta = 0.5$ and (c) $\delta = 0.7$. Here $\sigma_{Te} = 0.2, \sigma_e = 10, k = 0.2, l_x = 0.2, \theta = 5^\circ, \omega_0 = 0.03$.

(i) Ultra-Relativistic Case (figure 7): As $\sigma_{Te}$ increases from 0.1 to 0.3, the nature of the attractors and the position of the fixed points are influenced.

(ii) Weakly Relativistic Case (figure 8): Similar changes are observed with an increase in $\sigma_{Te}$, but the degree of separation of fixed points differs from the ultra-relativistic case.

Figures 9 and 10 depicts the effect of $\sigma_e$ (Rest to Fermi Energy Ratio):

(i) Ultra-Relativistic Case (figure 9): Increasing $\sigma_e$ from 5 to 15 shows significant movement of fixed points apart.

(ii) Weakly Relativistic Case (figure 10): Similar trends are observed, with fixed points shifting with increasing $\sigma_e$.

In figures 11 and 12 the effect of Wavenumber ($k$) is explained in:

(i) Ultra-Relativistic Case (figure 11): Increasing $k$ from 0.2 to 0.6 leads to the rapid movement of fixed points apart.

(ii) Weakly Relativistic Case (figure 12): Fixed points also move apart, but at a different rate compared to the ultra-relativistic case.

Figures 13 and 14 shows the effect of Directional Cosines ($l_x$):

(i) Ultra-Relativistic Case (figure 13): Variations in Directional Cosines ($l_x$) from 0.2 to 0.6 affect the strength of attractors without significantly altering the position of fixed points.

(ii) Weakly Relativistic Case (figure 14): Changes in $l_x$ show similar influences as in the ultra-relativistic case.

Figures 15 and 16 shows the interesting effect of Angle of Inclination ($\theta$):

(i) Ultra-Relativistic Case (figure 15): Variations in $\theta$ (3° to 7°) show noticeable impacts on the phase portraits, altering the positions and nature of fixed points.

(ii) Weakly Relativistic Case (figure 16): Similar effects are observed with variations in $\theta$.

Figures 17 and 18 shares information on the effect of Rotational Frequency ($\omega_0$):

(i) Ultra-Relativistic Case (figure 17): Increasing $\omega_0$ from 0.03 to 0.07 influences the formation and separation of fixed points.

(ii) Weakly Relativistic Case (figure 18): Changes in $\omega_0$ show similar impacts as in the ultra-relativistic case.

Figures 19 and 20 illustrates the effect of Heavy-to-Light Nuclear Charge Density Ratio ($\delta$):

(i) Ultra-Relativistic Case (figure 19): Variations in $\delta$ affect the phase portraits, influencing the formation of envelope solitons.

(ii) Weakly Relativistic Case (figure 20): Similar trends are observed with changes in $\delta$.

### 4.2. Summary of results of the dynamical system

The figures collectively illustrate the dependence of the NLSE dynamics on various plasma parameters. The ultra-relativistic, weakly relativistic, and classical cases exhibit different behaviors in terms of fixed points and limit cycles, influenced by parameters like $\sigma_{Te}$, $\sigma_e$, $k$, $l_x$, $\theta$, $\omega_0$ and $\delta$. These analyses are crucial for understanding the nonlinear structures in magneto-rotating stellar plasmas.

## 5. Conclusions

This theoretical work gives a qualitative understanding of the different nonlinear structures in the accretion discs of stars and other stellar bodies which rotates in a magnetised environment. We have carried out an elaborate mathematical and numerical analysis To maintain the features of the physical article we have not stuffed our manuscript with those mathematics. However parametric dependence has been shown though the phase portrait analysis. The envelop soliton part was has been augmented with a breather mode type of solution and the modulation instability has been discussed in the light of Benjamin-Feir Index. The importance of this work can be understood in the light of star formation. Envelop soliton formation in stars and proto-stars is a fascinating astrophysical phenomenon, occurring within the convective envelopes of these celestial bodies. These solitons are localized, stable waves that propagate through the envelope, influencing energy transport and internal dynamics. In stars, they play a crucial role in regulating heat transfer, impacting overall stellar evolution.

Proto-stars, being in the early stages of formation, exhibit envelop solitons that contribute to the accretion process and the establishment of stable structures. Understanding the intricate interplay of envelop solitons sheds light on the complex dynamics within stars and proto-stars, offering insights into the broader context of astrophysical processes. In this study, a warm degenerate magneto-rotating quantum plasma system was examined to understand the nonlinear properties of Nuclear Acoustic Envelop Solitary waves (NAESs). The system consisted of warm non-relativistic or ultra-relativistic electrons, non-degenerate light nuclei, and a static heavy nucleus, with rotation considered around the $z$-axis at a small speed. Various parameters such as degenerate electrons, warm degenerate parameter, rotational frequency, inclination angle, and the presence of a static heavy nucleus were investigated for their effects on NASWs' generation, propagation, and characteristics.

Key findings include: The presence of non-relativistic or ultra-relativistic electrons supports the existence and propagation of compressional NAESs. NAESs potential amplitude decreases with increased temperature in degenerate non-relativistic plasma, while it increases with temperature in the presence of ultra-relativistic electrons. Rotational frequency does not affect NAESs amplitude but decreases the potential width. NAESs width increases with the inclination angle of rotation. The presence of a static heavy nucleus modifies NAESs' features, with amplitude and width decreasing with increased heavy nucleus density and charge state. The study suggests applicability to hot white dwarfs and systems like neutron stars, broadening the investigation scope of degenerate magneto-rotating plasma systems. However, it did not explore non-planar NAESs potential or arbitrary amplitude NAESs. Additionally, quantum effects like Bohm term and spin effects were not considered, indicating potential avenues for further research.

## Acknowledgments

The authors would like to thank Dr Partha Sona Maji, Assistant professor, Department of Physics, Amity School of Applied Sciences, Amity University Kolkata, Newtown, Kolkata 700135, India for his inputs in addressing many of the concerns raised by the reviewers. Authors also thank the Institute of Natural Sciences and Applied Technology, Kolkata for providing infrastructure facilities to carry out the research.

## Data availability statement

No new data were created or analysed in this study.

## Appendix

### A.1. Normalization scheme

The normalization is carried out accordingly [22]:

$$\tilde{n}_l = \frac{n_l}{n_{l0}} \tag{A1}$$

$$\tilde{n}_h = \frac{n_h}{n_{h0}} \tag{A2}$$

$$\tilde{n}_e = \frac{n_e}{n_{e0}} \tag{A3}$$

$$\tilde{u}_l = \frac{u_l}{c_l} \tag{A4}$$

$$\tilde{\omega}_r = \frac{\omega_r}{\omega_{pl}} \tag{A5}$$

$$\tilde{\omega}_c = \frac{\omega_c}{\omega_{pl}} \tag{A6}$$

$$x(\tilde{y}, z) = \frac{x(y, z)}{\lambda_{Dl}} \tag{A7}$$

$$\tilde{t} = t \times (\omega_{pl}^{-1}) \tag{A8}$$

$$\tilde{\phi} = \frac{e\phi}{k_e n_{e0}^{\gamma-1}} \tag{A9}$$

with $\omega_{pl} = \sqrt{\frac{4\pi n_{l0} Z_l^2 e^2}{m_l}}$ as the light nucleus plasma frequency and $c_l = [k_e {n_{e0}}^{\gamma_e - 1}/m_l]^{1/2}$ as the light nuclear acoustic wave speed respectively.

$$k_{Te} = \frac{(2\sqrt{1+\sigma_e^2}(1+24\sigma_{Te}^2) - 3\sigma_e^2\sigma_{ke}^2)}{(2\sqrt{1+\sigma_e^2} - 3\sigma_e^2\sigma_{ke}^2)}, \tag{A10}$$

where other parameters are defined as:

$$\sigma_e = m_e c^2/\varepsilon_{Fe} \tag{A11}$$

$$\sigma_{Te} = k_B T_e/\varepsilon_{Fe} \tag{A12}$$

$$\sigma_{ke}^2 = \sqrt{1+\sigma_e^2} + \sigma_e^2 \log\frac{\sigma_e}{1+\sqrt{1+\sigma_e^2}} \tag{A13}$$

$k_B$, $\varepsilon_{Fe}$, $T_e$, and $1/\sigma_e$ represent the Boltzmann constant, Fermi energy of the degenerate electrons, Temperature of degenerate electrons, and relativity parameter respectively.

Note: When $\sigma_e \gg 1$ and $\gamma_e = 5/3$, the equation characterizes a warm non-relativistic degenerate plasma state. Conversely, to depict an ultra-relativistic degenerate plasma state, one should consider $\sigma_e \ll 1$ and $\gamma_e = 4/3$ in the Chandrasekhar equation of state [22]. It is evident that, for $k_{Te} = 1$, corresponding to zero temperature conditions ($T_e = 0$ and $\sigma_{Te} = 0$), the electron number density equation simplifies to the cold degeneracy limit. In the case of $k_{Te} = 1$ and $\gamma_e = 1$ (representing a relativistic plasma system), the electron number density adheres to the conventional Maxwell-Boltzmann velocity distribution function.

### A.2. Set of normalized governing equations in the scalar form

$$\frac{\partial n_l}{\partial t} + \frac{\partial}{\partial x}(n_l u_{lx}) + \frac{\partial}{\partial z}(n_l u_{lz}) = 0, \tag{A14}$$

$$\frac{\partial u_{lx}}{\partial t} + \left(u_{lx}\frac{\partial}{\partial x} + u_{lz}\frac{\partial}{\partial z}\right)u_{lx} + \frac{\partial \phi}{\partial x} - u_{ly}(\omega_{cl} + 2\omega_0 \sin\theta) = 0 \tag{A15}$$

$$\frac{\partial u_{ly}}{\partial t} + \left(u_{lx}\frac{\partial}{\partial x} + u_{lz}\frac{\partial}{\partial z}u_{ly}\right)u_{ly} + u_{lx}\omega_{cl} + 2\omega_0(u_{lx}\cos\theta - u_{lz}\sin\theta) = 0 \tag{A16}$$

$$\frac{\partial u_{lz}}{\partial t} + \left(u_{lx}\frac{\partial}{\partial x} + u_{lz}\frac{\partial}{\partial z}\right)u_{lz} + \frac{\partial \phi}{\partial z} + 2u_{ly}\omega_0 \sin\theta = 0 \tag{A17}$$

$$\left(\frac{\partial^2}{\partial x^2} + \frac{\partial^2}{\partial z^2}\right)\phi = (1+\delta)n_e - n_l - \delta. \tag{A18}$$

## ORCID iDs

Swarniv Chandra https://orcid.org/0000-0001-9410-1619
Gobinda Manna https://orcid.org/0000-0001-9252-9224
Deepsikha Mahanta https://orcid.org/0009-0000-5855-2279

## References

[1] Bally J 2007 *Astrophys. Space Sci.* **311** 15–24
[2] Woosley S E and Heger A 2006 *AIP Conf. Proc.* **836** 398–407
[3] Wang L and Wheeler J C 2008 *Annu. Rev. Astron. Astrophys.* **46** 433–74
[4] Kargaltsev O, Pavlov G, Teter M and Sanwal D 2003 *New Astron. Rev.* **47** 487–90
[5] Durant M, Kargaltsev O, Pavlov G G, Kropotina J and Levenfish K 2013 *Astrophys. J.* **763** 72
[6] Morris M 1987 *Publ. Astron. Soc. Pac.* **99** 1115
[7] Sahai R and Trauger J T 1998 *Astron. J* **116** 1357
[8] Bujarrabal V, Castro-Carrizo A, Alcolea J and Sánchez Contreras C 2001 *A&A* **377** 868–97
[9] Guerrero M A, Rechy-García J S and Ortiz R 2020 *Astrophys. J.* **890** 50
[10] de Gouveia Dal Pino E M 2005 *Adv. Space Res.* **35** 908–24
[11] Romero G E, Boettcher M, Markoff S and Tavecchio F 2017 *Space Sci. Rev.* **207** 5–61
[12] Corbel S 2010 *Proc. Int. Astron. Union* **6** 205–14
[13] Jiménez-Rosales A and Dexter J 2018 *Mon. Not. R. Astron. Soc.* **478** 1875–83
[14] Obregon M and Stepanyants Y A 1998 *Phys. Lett.* A **249** 315–23
[15] Sultana S and Schlickeiser R 2018 *Phys. Plasmas* **25** 022110
[16] Abdikian A, Tamang J and Saha A 2021 *Phys. Scr.* **96** 095605
[17] Chandra S *et al* 2024 *IEEE Trans. Plasma Sci.* 1–14
[18] Mamun A A, Amina M and Schlickeiser R 2016 *Phys. Plasmas* **23** 094503
[19] Shapiro S L and Teukolsky S A 2008 *Black Holes, White Dwarfs, and Neutron Stars: The Physics of Compact Objects* (Wiley)
[20] Zaman D, Amina M, Dip P and Mamun A 2017 *The European Physical Journal Plus* **132** 1–8
[21] Dasgupta S and Karmakar P K 2021 *Sci. Rep.* **11** 19126
[22] Akter J and Mamun A A 2022 *Fluids* **7** 305

[23] Farooq M, Mushtaq A and Qasim J 2019 *Contrib. Plasma Phys.* **59** 122–35
[24] Ghosh M, Sharry K, Dutta D and Chandra S 2021 *The African Review of Physics* **15** 63
[25] Hussain S, Ur-Rehman H and Mahmood S 2014 *Astrophys. Space Sci.* **350** 185–90
[26] Karmakar P K and Das P 2018 *Phys. Plasmas* **25** 082902
[27] Singh K, Sethi P and Saini N S 2019 *Phys. Plasmas* **26** 092104
[28] Wang H, Du J and Guo R 2022 *Phys. Scr.* **98** 015204
[29] Abraham J W and Bonitz M 2014 *Contrib. Plasma Phys.* **54** 27–99
[30] Dey A, Chandra S, Das C, Mandal S and Das T 2022 *IEEE Trans. Plasma Sci.* **50** 1557–64
[31] Manna G, Dey S, Goswami J, Chandra S, Sarkar J and Gupta A 2022 *IEEE Trans. Plasma Sci.* **50** 1464–76
[32] Das C, Chandra S, Saha A and Chatterjee P 2024 *IEEE Trans. Plasma Sci.* 1–9
[33] Chandra S, Das C, Sarkar J and Chowdhari C 2023 *Pramana-Journal of Physics* **98**